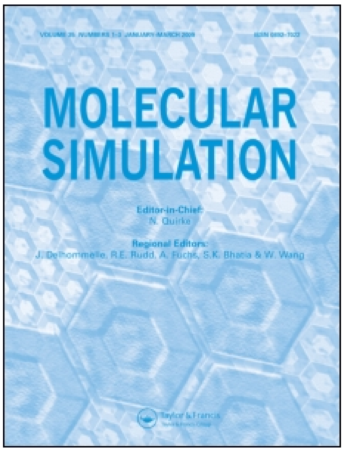

Molecular Simulation
Publication details, including instructions for authors and subscription information:
http://www.informaworld.com/smpp/title~content=t713644482

A density functional theory for Yukawa chain fluids in a nanoslit

Yu Liu[a]; Xueqian Chen[a]; Honglai Liu[a]; Ying Hu[a]; Jianwen Jiang[b]
[a] State Key Laboratory of Chemical Engineering, Department of Chemistry, East China University of Science and Technology, Shanghai, China [b] Department of Chemical and Biomolecular Engineering, National University of Singapore, Singapore

First published on: 22 January 2010

To cite this Article Liu, Yu , Chen, Xueqian , Liu, Honglai , Hu, Ying and Jiang, Jianwen(2010) 'A density functional theory for Yukawa chain fluids in a nanoslit', Molecular Simulation, 36: 4, 291 — 301, First published on: 22 January 2010 (iFirst)

To link to this Article: DOI: 10.1080/08927020903348960

URL: http://dx.doi.org/10.1080/08927020903348960

Molecular Simulation
Vol. 36, No. 4, April 2010, 291–301

A density functional theory for Yukawa chain fluids in a nanoslit

Yu Liu[a], Xueqian Chen[a], Honglai Liu[a]*, Ying Hu[a] and Jianwen Jiang[b]

[a]*State Key Laboratory of Chemical Engineering, Department of Chemistry, East China University of Science and Technology, Shanghai 200237, China;* [b]*Department of Chemical and Biomolecular Engineering, National University of Singapore, 117576, Singapore*

(*Received 4 June 2009; final version received 16 September 2009*)

A weighted density functional theory is developed for Yukawa chain fluids confined in a nanoslit. The excess free-energy functional is separated into repulsive and attractive contributions. A simple Heaviside function is used as the weighting function to calculate the weighted density in both contributions. The excess free-energy functional of repulsive interaction is calculated by the equation of state developed by Liu et al., while the contribution to excess free-energy functional by attractive interaction is calculated using the statistical associating fluids theory for chain molecules with attractive potentials of variable range. For pure fluids, the predicted density profiles near the nanoslit wall are in good agreement with simulations. The effect of cut-off introduced in the weighting function for the attractive part is examined; in addition, the surface excess and partition coefficient are calculated. The density profiles are also predicted for mixtures of two Yukawa chain fluids with different chain lengths, hard-core diameters, fluid–fluid and wall–fluid interactions. This work reveals that it is important to decompose the excess free-energy functional into repulsive and attractive contributions, and a simple weighting function can be used for both contributions.

Keywords: density functional; Yukawa fluids; weighted density approximation; slit; confined space

1. Introduction

The properties of polymeric fluids confined in nanogeometries are of central importance in a wide variety of industrial applications, such as wetting [1], layering, capillary condensation, adsorption [2], etc. In nanopores or mesopores, fluids behave significantly different from bulk systems attributed to fluid–surface interactions and geometric constraints. A number of experimental, simulation and theoretical methods have been developed to study the adsorption and phase behaviour of fluids in nanospace. For example, grand canonical Monte Carlo (MC) simulation and isotension ensemble MC simulation have been used [3–9]. Simulations are efficient for short-chain molecules; however, they are computationally expensive for long-chain molecules and for systems at high densities. In this regard, density functional theory (DFT) is robust to study long-chain molecules and complicated systems, including microscopic structural and thermodynamic properties of bulk and inhomogeneous fluids.

It is formidable to derive the exact expression of excess free-energy functional in DFT for most systems; as a consequence, approximations are required at various levels. For example, the local density approximation [4,10], the functional expand approximation [11,12], the fundamental measure theory (FMT) [13–15], the bridge function-based DFT [16] and the weighted density approximation (WDA) [17–19] have been demonstrated effectively for different systems. Yethiraj and Woodward (YW) [17] proposed a simple and accurate DFT, which estimates the ideal-gas functional through single-chain simulation and the excess free-energy functional by WDA with a simple weighting function. This approach was subsequently improved by Yethiraj [18] by using a more sophisticated weighting function based on the Curtin–Ashcroft (CA) recipe [19].

For real fluids, DFT has been developed based on models with attractive interactions, such as hard-core square-well (SW) model, hard-core attractive Yukawa (HCAY) model and Lennard-Jones (LJ) model. Patra and Yethiraj [20] employed the YW theory along with a van der Waals approximation to study the effect of attractions on polymers confined between surfaces. They mimicked polymers as Yukawa chain fluids and obtained accurate results at high densities and high temperatures. Subsequently, they further improved [21] the theory by using WDA and the direct correlation function (DCF) separately in repulsive and attractive interactions. The DCF was obtained from the polymer-reference-interaction-site model (PRISM) [22]. Goel and Patra [23] applied the YW theory based on the CA recipe and DCF from the PRISM, in addition to the mean spherical approximation (MSA) for Yukawa chains. The predicted results are accurate at weak fluid–fluid

*Corresponding author. Email: hlliu@ecust.edu.cn

ISSN 0892-7022 print/ISSN 1029-0435 online

DOI: 10.1080/08927020903348960
http://www.informaworld.com

attraction upon comparison with simulation data. Using two Heaviside functions to describe the excess free-energy functional, respectively, for repulsive and attractive contributions, Ye et al. [24,25] examined pure and mixed SW chains and obtained satisfactory results. del Río et al. [26] studied a molecular model consisting of parallel hard oblate ellipsoids with superimposed SW interactions using the WDA for hard-sphere part and mean-field theory for SW potential. Li and Wu [27] investigated the structural and thermodynamic properties of concentrated electrolyte and neutral component mixtures. By combining FMT and mean-field theory, Li et al. [28] developed a non-local DFT for polymeric fluids consisting of freely jointed LJ chains. Ayadim and Amokrane [29] studied the fluid–fluid binodals of highly asymmetric binary hard-sphere mixtures using FMT and MSA. Martínez-Ratón et al. [30] introduced a fundamental measure DFT to study the mixtures of parallel hard cylinders. Peng and Yu [31] studied LJ fluids using modified FMT (MFMT) and WDA theory to calculate the repulsive and attractive interactions, respectively. Karanikas et al. [32] studied Yukawa fluids using DFT, integral equation and molecular simulation. WDA and mean-field theory were also combined together by Kim and Lee [33] to investigate polymer melts at interfaces. Yang and Yang [34] studied the structure of hard-core Yukawa fluid mixtures near a semi-permeable membrane using FMT and mean-field theory. Recently, Wu et al. [35–37] have extended DFT for polyelectrolyte at interfaces.

In this work, we employ WDA to study the structural and thermodynamic properties of Yukawa chain fluids confined in an attractive nanoslit. The excess free-energy functional is separated into repulsive and attractive contributions. Unlike most previous studies, a simple Heaviside function is used here as the weighting function for both repulsive and attractive contributions. Despite the simple expressions of the weighting function, the results are more accurate at both high and low temperatures. In Section 2, the DFT theory developed in this work is described in detail for pure Yukawa chain fluids and for mixtures. The predicted density profiles, surface excess and partition coefficient are presented in Section 3 and compared with the available simulation results. In addition, the effect of cut-off introduced as an adjustable parameter is examined. The concluding remarks are summarised in Section 4.

2. Theory

2.1 Pure component

We first consider a pure Yukawa chain fluid confined between two infinite parallel walls. The chain consists of m freely jointed tangential hard cores of diameter σ. The fluid–fluid site–site interaction $u_{\mathrm{ff}}(r)$ is modelled as a HCAY potential,

$$u_{\mathrm{ff}}(r)=\begin{cases}-\varepsilon_{\mathrm{ff}}\frac{\sigma}{r}\exp\left[-\kappa\left(\frac{r}{\sigma}-1\right)\right], & r>\sigma,\\ \infty, & r<\sigma,\end{cases}\tag{1}$$

where $\beta=1/k_{\mathrm{B}}T$, k_{B} is Boltzmann's constant, T is the absolute temperature and r denotes the distance between any two beads. The interaction $u_{\mathrm{wf}}(z)$ between the impenetrable walls and the fluid is

$$u_{\mathrm{wf}}(z)=\begin{cases}-\varepsilon_{\mathrm{wf}}\{\exp(-\kappa z/\sigma)+\exp[-\kappa(H-z)/\sigma]\}, & H>z>0,\\ \infty, & \text{elsewhere},\end{cases}\tag{2}$$

where H (set to 10 in this work) is the separation between the two walls, $\varepsilon_{\mathrm{wf}}$ and $\varepsilon_{\mathrm{ff}}$ are the strengths of wall–fluid and fluid–fluid interactions, respectively, and κ is the inverse range of the Yukawa potential (set to $\kappa=2.5$ in this work). All lengths are scaled by simply setting $\sigma=1$.

In DFT, one starts with an expression for the grand potential Ω as a functional of the density profile of the fluid,

$$\Omega[\rho_{\mathrm{M}}(R)]=F[\rho_{\mathrm{M}}(R)]+\int V_{\mathrm{ext}}(R)\rho_{\mathrm{M}}(R)\mathrm{d}R - \mu\int\rho_{\mathrm{M}}(R)\mathrm{d}R,\tag{3}$$

where $F[\rho_{\mathrm{M}}(R)]$ is the intrinsic Helmholtz free-energy functional, μ is the chemical potential, $R=\{r_1,\ldots,r_m\}$ denotes the position of m segments of a polymer chain, where r_i is the spatial position of the ith segment, $V_{\mathrm{ext}}(R)$ is the external field and $\rho_{\mathrm{M}}(R)$ is the molecular density.

The Helmholtz free-energy functional $F[\rho_{\mathrm{M}}(R)]$ can be expressed as the sum of an ideal $F^{\mathrm{id}}[\rho_{\mathrm{M}}(R)]$ and an excess part $F^{\mathrm{ex}}[\rho_{\mathrm{M}}(R)]$:

$$F[\rho_{\mathrm{M}}(R)]=F^{\mathrm{id}}[\rho_{\mathrm{M}}(R)]+F^{\mathrm{ex}}[\rho_{\mathrm{M}}(R)].\tag{4}$$

The ideal gas functional $F^{\mathrm{id}}[\rho_{\mathrm{M}}(R)]$ is given by

$$F^{\mathrm{id}}[\rho_{\mathrm{M}}(R)]=k_{\mathrm{B}}T\int\rho_{\mathrm{M}}(R)[\ln\rho_{\mathrm{M}}(R)-V_{\mathrm{intra}}(R)]\mathrm{d}R,\tag{5}$$

where $V_{\mathrm{intra}}(R)$ is the intramolecular interaction. The density profile and thermodynamic properties of the system are obtained by minimising Ω with respect to $\rho_{\mathrm{M}}(R)$ at equilibrium,

$$\delta\Omega[\rho_{\mathrm{M}}(R)]/\delta\rho_{M}(R)=0.\tag{6}$$

Then, we can obtain the density distribution

$$\rho_M(R) = \exp\left\{\beta\left(\mu - V_{\text{ext}}(R) - V_{\text{intra}}(R) - \frac{\delta F^{\text{ex}}[\rho_M]}{\delta\rho_M(R)}\right)\right\}. \tag{7}$$

The chain segment density $\rho(r)$ is related to the polymer molecule density distribution $\rho_M(R)$ via

$$\rho(r) = \int \sum_{i=1}^{m} \delta(r - r_i)\rho_M(R)\mathrm{d}R. \tag{8}$$

Combining Equations (7) and (8), we have

$$\rho(r) = \int \sum_{i=1}^{m} \delta(r - r_i) \exp\left\{\beta\left(\mu - V_{\text{ext}}(r) - V_{\text{intra}}(R) - \frac{\delta F^{\text{ex}}[\rho_M]}{\delta\rho_M(R)}\right)\right\}\mathrm{d}R \tag{9}$$

and

$$\frac{\delta F^{\text{ex}}[\rho_M]}{\delta\rho_M(R)} = \sum_{i=1}^{m} \int \frac{\delta F^{\text{ex}}[\rho_M]}{\delta\rho(r')}\delta(r' - r_i)\mathrm{d}r'. \tag{10}$$

Following Yethiraj et al. [17,20], we separate the excess Helmholtz free-energy functional into two parts,

$$F^{\text{ex}}[\rho_M(R)] = F^{\text{ex}}_{\text{hs}}[\rho_M(R)] + F^{\text{ex}}_{\text{attr}}[\rho_M(R)], \tag{11}$$

where the subscript 'hs' denotes hard-sphere and 'attr' denotes attractive contribution. We employ WDA for both hard-sphere and attractive parts as Ye et al. [24, 25] who studied SW chain fluids.

$$F^{\text{ex}}_{\text{hs}}[\rho_M] = \int \rho(r) f_{\text{hs}}[\bar{\rho}_{\text{hs}}(r)]\mathrm{d}r, \tag{12a}$$

$$F^{\text{ex}}_{\text{attr}}[\rho_M] = \int \rho(r) f_{\text{attr}}[\bar{\rho}_{\text{attr}}(r)]\mathrm{d}r, \tag{12b}$$

where $f_{\text{hs}}(\rho)$ is the excess Helmholtz free-energy density due to hard-sphere contribution, while $f_{\text{attr}}(\rho)$ is due to attractive contribution. The equation of state (EOS) of Liu and Hu [38] is used to calculate the excess Helmholtz free energy of the hard-sphere part, while the statistical associating fluids theory for chain molecules with attractive potentials of variable range (SAFT-VR) is used to calculate the attractive part [39]. The expression for the SAFT-VR is given in the appendix. The weighted density $\bar{\rho}$ is given by

$$\bar{\rho}_{\text{hs}}(r) = \int \rho(r') w_{\text{hs}}(|r - r'|)\mathrm{d}r', \tag{13a}$$

$$\bar{\rho}_{\text{attr}}(r) = \int \rho(r') w_{\text{attr}}(|r - r'|)\mathrm{d}r', \tag{13b}$$

where $w_{\text{hs}}(r)$ and $w_{\text{attr}}(r)$ are unitary weight functions which satisfy

$$\int w_{\text{hs}}(r)\mathrm{d}r = \int w_{\text{attr}}(r)\mathrm{d}r = 1. \tag{14}$$

For the hard-sphere part, it is convenient to employ a simple Heaviside function as the weighting function,

$$w_{\text{hs}}(r) = 3\Theta(\sigma - r)/(4\pi\sigma^3). \tag{15}$$

The weighting function for the attractive part is not readily available. In this work, we introduce a simple Heaviside function, as used for the hard-sphere part, for the attractive part by truncating the weighting function at r_{cut},

$$w_{\text{attr}}(r) = 3\Theta(r_{\text{cut}} - r)/(4\pi r_{\text{cut}}^3). \tag{16}$$

The truncated radius r_{cut} represents the length of correlation between particles and is set as a constant ($r_{\text{cut}} = 5\sigma$) in most of our calculations, and the effect of r_{cut} will be discussed below.

With the two weighting functions and the excess Helmholtz free energy, Equations (9) and (10) can be converted to

$$\rho(r) = \int \sum_{i=1}^{m} \delta(r - r_i) \exp\left[\beta\left(\mu - V_{\text{ext}}(r) - V_{\text{intra}}(R) - \sum_{j=1}^{m}(\lambda_{\text{hs}}(r_j) + \lambda_{\text{attr}}(r_j))\right)\right]\mathrm{d}R, \tag{17}$$

where

$$\begin{aligned}\lambda_{\text{hs}}(r) &= \beta f_{\text{hs}}[\bar{\rho}_{\text{hs}}(r)] + \int \rho(r') \times \frac{\partial \beta f_{\text{hs}}[\bar{\rho}_{\text{hs}}(r)]}{\partial \bar{\rho}_{\text{hs}}(r')}\frac{\delta\bar{\rho}_{\text{hs}}(r')}{\delta\rho(r)}\mathrm{d}r' \\ &= \beta f_{\text{hs}}[\bar{\rho}_{\text{hs}}(r)] + \int \rho(r') w_{\text{hs}}(|r' - r|) \times \frac{\partial \beta f_{\text{hs}}[\bar{\rho}_{\text{hs}}(r)]}{\partial \bar{\rho}_{\text{hs}}(r')}\mathrm{d}r',\end{aligned} \tag{18a}$$

and

$$\lambda_{\text{attr}}(r) = \beta f_{\text{attr}}[\bar{\rho}_{\text{attr}}(r)] + \int \rho(r') \times \frac{\partial \beta f_{\text{attr}}[\bar{\rho}_{\text{attr}}(r)]}{\partial \bar{\rho}_{\text{attr}}(r')} \frac{\delta \bar{\rho}_{\text{attr}}(r')}{\delta \rho(r)} \mathrm{d}r' = \beta f_{\text{attr}}[\bar{\rho}_{\text{attr}}(r)] + \int \rho(r') w_{\text{attr}}(|r' - r|) \times \frac{\partial \beta f_{\text{attr}}[\bar{\rho}_{\text{attr}}(r)]}{\partial \bar{\rho}_{\text{attr}}(r')} \mathrm{d}r'. \tag{18b}$$

The intramolecular interaction potential $V_{\text{intra}}(R)$ in Equation (17) can be obtained by the single-chain simulation [17] or numerical calculation [40,41]. In this work, the numerical method is adopted and the intramolecular interaction potential is approximated as

$$V_{\text{intra}}(R) \approx \sum_{i=1}^{m-1} v_{\text{b}}(|r_{i+1} - r_i|), \tag{19}$$

where v_{b} is the bonding potential. As we consider the polymers as tangentially connected Yukawa chains, the bonding potential can be written as

$$\exp(-\beta v_{\text{b}}(|r - r'|)) = \frac{1}{4\pi\sigma^2} \delta(|r - r'| - \sigma). \tag{20}$$

By substituting Equations (19) and (20) into Equation (17), we have

$$\rho(r) = \exp(\beta\mu) \sum_{i=1}^{m} \exp(-\beta\Psi_i(r)) \times \int \frac{\delta(|r_2 - r_1| - \sigma)}{4\pi\sigma^2} \exp(-\Psi_1(r_1)) \mathrm{d}r_1 \cdots \int \frac{\delta(|r - r_{i-1}| - \sigma)}{4\pi\sigma^2} \exp(-\Psi_{i-1}(r_{i-1})) \mathrm{d}r_{i-1} \times \int \frac{\delta(|r_{i+1} - r| - \sigma)}{4\pi\sigma^2} \exp(-\Psi_{i+1}(r_{i+1})) \mathrm{d}r_{i+1} \cdots \int \frac{\delta(|r_m - r_{m-1}| - \sigma)}{4\pi\sigma^2} \exp(-\Psi_m(r_m)) \mathrm{d}r_m, \tag{21}$$

in which

$$\Psi_i(r_i) = V_{\text{ext}}(r_i) + \lambda_{\text{hs}}(r_i) + \lambda_{\text{attr}}(r_i). \tag{22}$$

For the external potential, which is a function only of the z-coordinate, the density distribution depends only on the z-coordinate. Then, Equations (21) can be simplified as

$$\rho(z) = \exp(\beta\mu_{\text{M}}) \sum_{i=1}^{m} \exp(-\beta\Psi_i(z)) G_{\text{L}}^i(z) G_{\text{R}}^i(z), \tag{23}$$

in which

$$G_{\text{L}}^i(z) = \frac{1}{2\sigma} \int_{\max(0, z-\sigma)}^{\min(H\sigma, z+\sigma)} \mathrm{d}z' \exp(-\beta\Psi_{i-1}(z')) G_{\text{L}}^{i-1}(z'), \tag{24a}$$

$$G_{\text{R}}^j(z) = \frac{1}{2\sigma} \int_{\max(0, z-\sigma)}^{\min(H\sigma, z+\sigma)} \mathrm{d}z' \exp(-\beta\Psi_{j+1}(z')) G_{\text{R}}^{j+1}(z'), \tag{24b}$$

where $i = 2, \ldots, m$ and $j = 1, \ldots, m-1$, with $G_{\text{L}}^1(z) = 1$ and $G_{\text{R}}^m(z) = 1$.

2.2 Mixtures

To calculate the cross-parameters for mixtures, the Lorentz–Berthelot combining rules, $\varepsilon_{\text{AB}} = \sqrt{\varepsilon_{\text{AA}}\varepsilon_{\text{BB}}}$ and $\sigma_{\text{AB}} = (\sigma_{\text{AA}} + \sigma_{\text{BB}})/2$, are used. The excess Helmholtz free energy can also be separated into two parts similar to Equation (11), and WDA is used for both parts,

$$F_{\text{hs}}^{\text{ex}}[\rho_{\text{M}}] = \sum_{i=1}^{K} \int \rho_i(r) f_{\text{hs}}[\bar{\rho}_{\text{hs},1}^{(i)}(r), \ldots, \bar{\rho}_{\text{hs},K}^{(i)}(r)] \mathrm{d}r, \tag{25a}$$

$$F_{\text{attr}}^{\text{ex}}[\rho_{\text{M}}] = \sum_{i=1}^{K} \int \rho_i(r) f_{\text{attr}}[\bar{\rho}_{\text{attr},1}^{(i)}(r), \ldots, \bar{\rho}_{\text{attr},K}^{(i)}(r)] \mathrm{d}r, \tag{25b}$$

with

$$f_{\text{hs}} = F_{\text{hs}}^{\text{ex}}/N_{\text{s}}, \tag{26a}$$

$$f_{\text{attr}} = F_{\text{attr}}^{\text{ex}}/N_{\text{s}}, \tag{26b}$$

where N_{s} denotes the segment density of all fluids, and $F_{\text{hs}}^{\text{ex}}$ and $F_{\text{attr}}^{\text{ex}}$ are the excess Helmholtz free energy for homogeneous fluids. The weighted density in (25a) and (25b) is represented by

$$\bar{\rho}_{\text{hs},j}^{(i)}(r) = \int \rho_j(r') w_{\text{hs}}^{(i,j)}(|r - r'|) \mathrm{d}r', \tag{27a}$$

$$\bar{\rho}_{\text{attr},j}^{(i)}(r) = \int \rho_j(r') w_{\text{attr}}^{(i,j)}(|r - r'|) \mathrm{d}r'. \tag{27b}$$

The weighting function is denoted as

$$w_{\text{hs}}^{(i,j)}(r) = 3\Theta(\sigma_{i,j} - r)/(4\pi\sigma_{i,j}^3), \tag{28a}$$

$$w_{\text{attr}}^{(i,j)}(r) = 3\Theta(r_{\text{cut}\,(i,j)} - r)/(4\pi r_{\text{cut}\,(i,j)}^3). \tag{28b}$$

Similar to pure fluids, $r_{\text{cut}(i,j)}$ is defined as $r_{\text{cut}(i,j)} = 5\sigma_{i,j}$. With the proper approximation for excess Helmholtz free

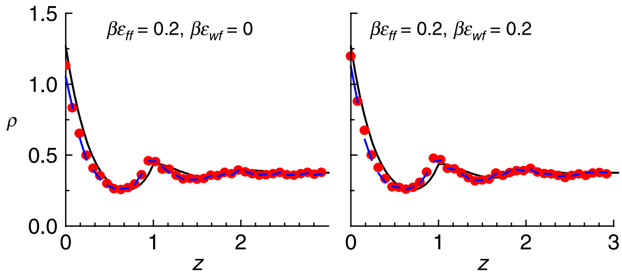

Figure 1. Density profiles of 5-mer near the nanoslit wall at $\eta = 0.4$. Solid lines, our DFT predictions; dashed lines, DFT predictions of Goel et al. [23]; symbols, MC data [23].

energy, the grand potential is similar to Equation (3),

$$\Omega[\rho_{\mathrm{M}}] = F_{\mathrm{int}}[\rho_{\mathrm{M}}] + \sum_{i=1}^{K} \int V_{\mathrm{ext}}^{(i)}(R_i)\rho_{\mathrm{M}}^{(i)}(R_i)\mathrm{d}R - \mu_i \int \rho_{\mathrm{M}}^{(i)}(R_i)\mathrm{d}R. \quad (29)$$

The density profiles of component *i* can be calculated from

$$\delta\Omega/\delta\rho_{\mathrm{M}}^{(i)}(R) = 0. \quad (30)$$

3. Results and discussion

3.1 Density profiles

The density profiles of polymeric fluids confined in a nanoslit are governed by the counterbalance among configurational entropy, packing effect and wall–fluid interaction (u_{wf}). Figure 1 shows the density profiles of 5-mer at packing fraction $\eta = 0.4$, fluid–fluid interaction $\varepsilon_{\mathrm{ff}} = 0.2$ and wall–fluid interaction $\varepsilon_{\mathrm{wf}} = 0$ and 0.2. Despite the use of a simple weighting function, the predictions from our DFT are close to Goel et al.'s theoretical results. Both are in good agreement with the simulation data. For this short-chain fluid at a high packing fraction, chains are preferentially packed near the wall to facilitate efficient packing. The density profiles at two different $\varepsilon_{\mathrm{wf}}$ are indiscernible, implying the negligible effect of $\varepsilon_{\mathrm{wf}}$ on the fluid structure in this case.

Figure 2 shows the density profiles of 10-mer near the nanoslit wall at packing fraction $\eta = 0.2$ with weak ($\varepsilon_{\mathrm{ff}} = 0.2$) and strong ($\varepsilon_{\mathrm{ff}} = 0.5$) fluid–fluid interactions. With the increasing chain length from 5 to 10, the configurational entropy becomes a dominator. As a consequence, depletion is observed in all the cases for 10-mer with the density near the wall lower than in the bulk. Nevertheless, the degree of depletion is more or less influenced by both $\varepsilon_{\mathrm{ff}}$ and $\varepsilon_{\mathrm{wf}}$. At $\varepsilon_{\mathrm{ff}} = 0.2$, the density near the wall is not significantly reduced compared to the bulk density, and it becomes slightly higher upon increasing $\varepsilon_{\mathrm{wf}}$ from 0 to 0.2. Our DFT predictions of density profiles agree well with the simulation data and are better than Goel et al.'s work, particularly near the wall. With a strong fluid–fluid interaction ($\varepsilon_{\mathrm{ff}} = 0.5$), the density near the wall is much lower than in the bulk and rises appreciably when $\varepsilon_{\mathrm{wf}}$ increases from 0 to 0.5. Again, the predictions of our DFT are in good accordance with the simulation data. Goel et al.'s predictions fail to capture the trend in profile, though a sophisticated weighting function was used. This is because the MSA used by Goel et al. is not very accurate in this case. We can infer that a more complicated weighting function for hard-sphere contribution does not necessarily lead to accurate predictions when the fluid–fluid attractive interaction is strong. The WDA used in our DFT appears to be a simple and reasonable approximation.

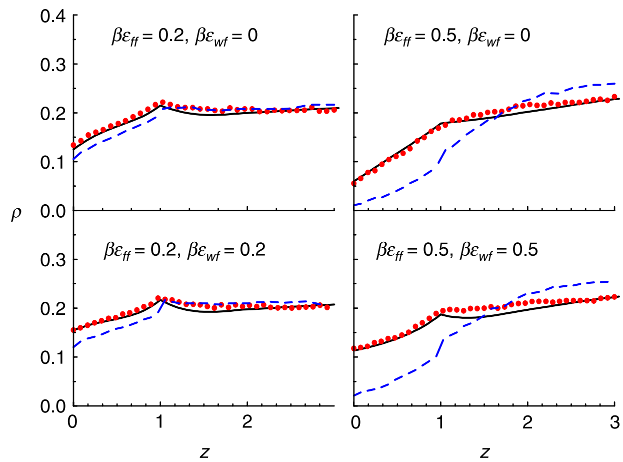

Figure 2. Density profiles of 10-mer near the nanoslit wall at $\eta = 0.2$. Solid lines, our DFT predictions; dashed lines, DFT predictions of Goel et al. [23]; symbols, MC data [23].

The density profiles of 20-mer at $\eta = 0.1$, $\varepsilon_{\mathrm{ff}} = 0.2$ and $\varepsilon_{\mathrm{wf}} = 0$ and 0.2 are shown in Figure 3. Compared to 10-mer in Figure 2, the configuration of entropy plays a more dominant role in determining the structure, and the depletion of chain near the wall is more pronounced.

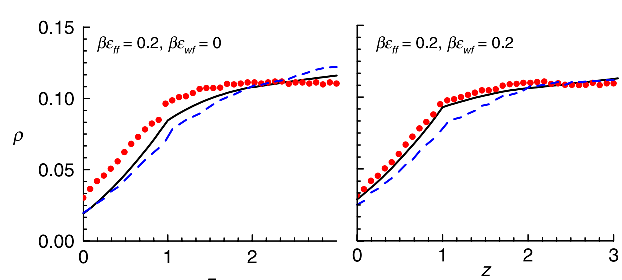

Figure 3. Density profiles of 20-mer near the nanoslit wall at $\eta = 0.1$. Solid lines, our DFT predictions; dashed lines, DFT predictions of Goel et al. [23]; symbols, MC data [23].

Our DFT performs better than Goel et al.'s work; however, the predictions near the hard wall ($\varepsilon_{wf} = 0$) are less perfect for 20-mer. This implies that the theory needs to be improved for long-chain fluids.

3.2 Effect of r_{cut}

In the developed DFT, an adjustable parameter cut-off r_{cut} has been introduced in the weighting function for the attractive part w_{attr} and chosen to be $r_{cut} = 5\sigma$. To examine the effect of r_{cut}, the average deviation of density (δ_{av}) and the deviation of contact density (δ_c) from the simulation were estimated,

$$\delta_{av} = \sqrt{\frac{1}{H}\int_0^H dz[\eta(z) - \eta_{MC}(z)]^2/\eta_{bulk}^2}, \tag{31}$$

$$\delta_c = |\eta(0) - \eta_{MC}(0)|/\eta_{bulk} \tag{32}$$

Figure 4 shows δ_{av} and δ_c at different r_{cut} for 5-, 10- and 20-mer, as discussed in Figures 1–3. Apparently, the best r_{cut} is pertinent to the correlation between fluids. For 5-mer at a high packing fraction $\eta = 0.4$ and the correlation being strong, δ_{av} is nearly a constant and δ_c increases with r_{cut}. In this case, a small r_{cut} gives better results. For 10-mer at a moderate packing fraction $\eta = 0.2$, δ_{av} is nearly a constant at $\varepsilon_{ff} = 0.2$, but exhibits a minimum at $\varepsilon_{ff} = 0.5$; δ_c also shows the minimum regardless of the value of ε_{ff}. Therefore, a moderate r_{cut} should be chosen. In markedly contrast with this, for 20-mer at a low packing fraction $\eta = 0.1$ with weak correlation, both δ_{av} and δ_c monotonically decrease with r_{cut}; and consequently, a large r_{cut} is better. Overall, $r_{cut} = 3–6$ appears to be appropriate, which gives δ_{av} under 0.1 and δ_c around 0.2. In most of our calculations, $r_{cut} = 5$ has been simply used.

3.3 Surface excess and partition coefficient

The thermodynamic properties including surface excess and partition coefficient are estimated. The surface excess is defined as [42]

$$\Gamma = \int_0^{Z_{bulk}} (\rho(z) - \rho_{bulk})dz, \tag{33}$$

where Z_{bulk} is the distance sufficiently far from the wall and approaches the bulk phase.

The partition coefficient is defined as

$$K = \frac{\rho_{av}}{\rho_{bulk}}, \tag{34}$$

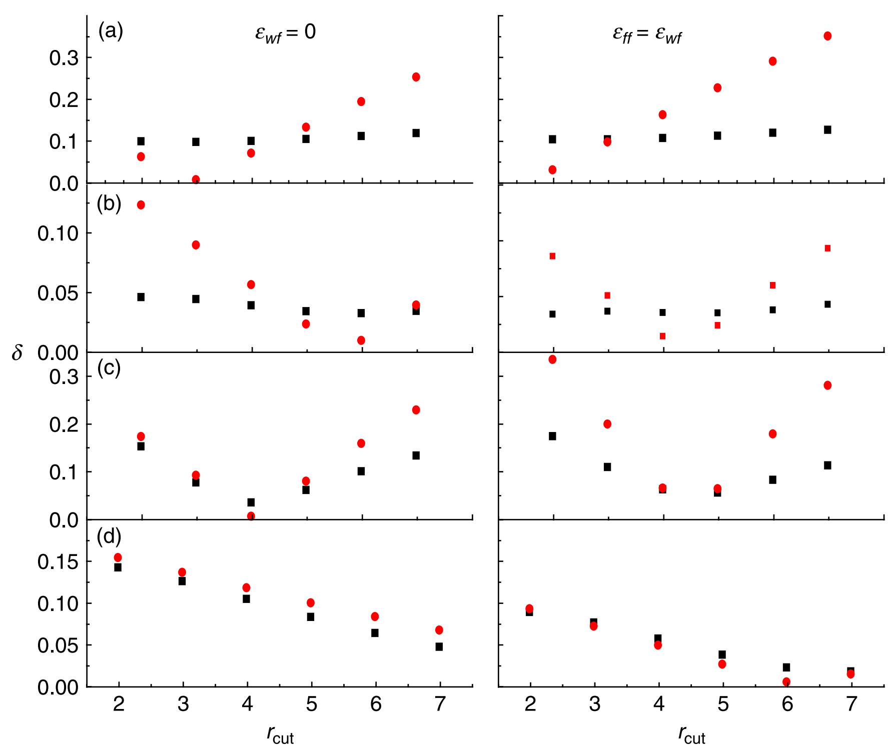

Figure 4. Average deviations (squares) and deviations of contact density (circles) from MC data at different r_{cut}: (a) 5-mer, $\eta = 0.4$, $\beta\varepsilon_{ff} = 0.2$, (b) 10-mer, $\eta = 0.2$, $\beta\varepsilon_{ff} = 0.2$, (c) 10-mer, $\eta = 0.2$, $\beta\varepsilon_{ff} = 0.5$ and (d) 20-mer, $\eta = 0.1$, $\beta\varepsilon_{ff} = 0.2$.

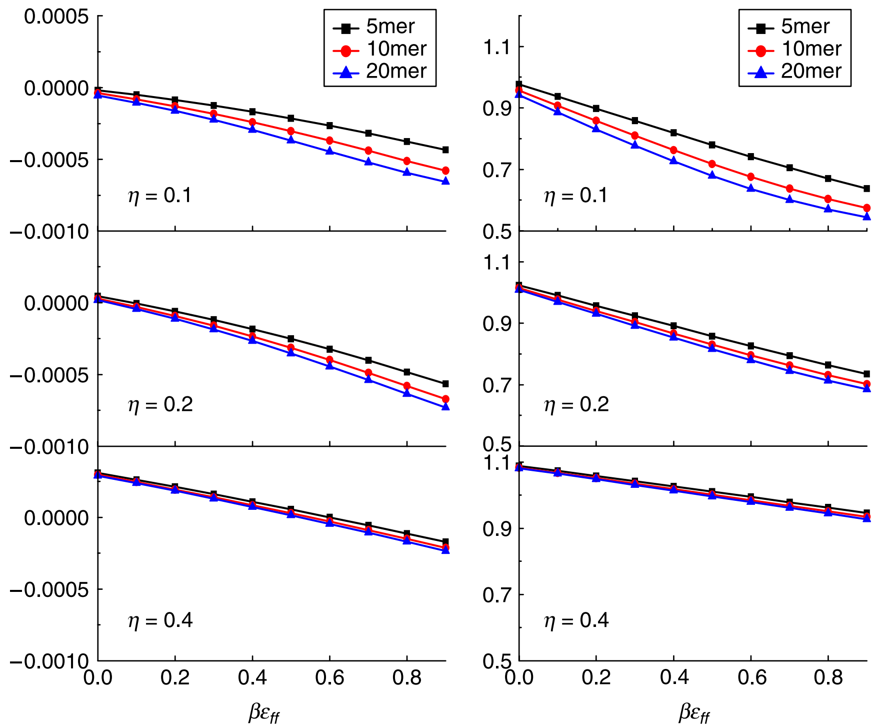

Figure 5. Surface excess Γ (left) and partition coefficient *K* (right) as a function of temperature ($\beta\varepsilon_{\rm ff} = 1/T^*$) for different chain lengths and packing fractions.

where $\rho_{\rm av}$ is the average density in the nanoslit:

$$\rho_{\rm av} = \frac{1}{H}\int_0^H \rho(z){\rm d}z. \tag{35}$$

Figure 5 shows the surface excess and partition coefficient for 5-, 10- and 20-mer as a function of temperature (represented by $\beta\varepsilon_{\rm ff} = 1/T^*$) at different densities. Both surface excess and partition coefficient decrease with increasing $\varepsilon_{\rm ff}$. This is because the fluid–fluid interaction is enhanced at high $\varepsilon_{\rm ff}$ and chains tend to reside in the bulk instead of being in the nanoslit. Among the three densities $\eta = 0.1$, 0.2 and 0.4 considered, negative surface excess is observed at $\eta = 0.1$ and 0.2 due to the dominant configurational entropy at low density. However, at $\eta = 0.4$, the surface excess is positive at low $\varepsilon_{\rm ff}$ due to the packing effect, which leads to the preferential laying of chain near the surface. In the same spirit, the partition coefficient is less than unity at $\eta = 0.1$ and 0.2, but turns to the opposite at $\eta = 0.4$ when $\varepsilon_{\rm ff}$ is low. In addition, we can see that both the surface excess and the partition coefficient drop with increasing chain length as the configurational entropy of longer chain is stronger, which facilitates chains to stay in the bulk.

Figure 6 shows the surface excess and partition coefficient as a function of density η at a given $\varepsilon_{\rm ff} = \varepsilon_{\rm wf} = 0.2$. With increasing density, the surface excess initially decreases at low density ($\eta < 0.1$) and then increases. At low density, the fluid–fluid interaction is insignificant and the configurational entropy plays a key role. The fluid chains tend to stay in the bulk to gain more configurational entropy. With a small increase in density, the fluid–fluid attractive interaction causes a greater number of chains to stay in the bulk and thus the surface excess decreases. Nevertheless, at sufficiently high density, the packing effect starts to come into play and chains are closer to the surface; as a consequence, the surface excess rises. Similar to Figure 5, the surface excess and partition coefficient decrease with increasing chain length because of the configurational entropy effect. A closer look over Figures 5 and 6 shows that the surface excess and partition coefficient of different chain lengths tend to converge at high density. The reason is that chains cannot move freely in a crowded environment and the configurational entropy and packing effect are approximately in the same magnitude at a high density, and the chain length effect is negligible.

3.4 *Density profiles in mixtures*

We examine the density profiles in mixtures of two Yukawa chain fluids A and B. The two fluids have the same segment density, but differ in fluid–fluid interaction, chain length, hard-sphere diameter and wall–fluid interaction, respectively. At different fluid–fluid interactions

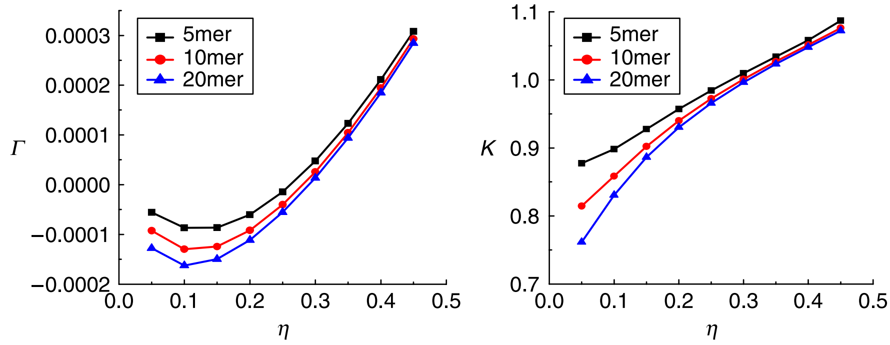

Figure 6. Surface excess Γ (left) and partition coefficient K (right) as a function of density η at $\varepsilon_{ff} = \varepsilon_{wf} = 0.2$ and different chain lengths.

as shown in Figure 7, with decreasing ε_{AA} and increasing ε_{BB}, A appears being proximal to the wall and its density rises near the wall. In contrast, B prefers to stay in the bulk and the laying structure of B tends to diminish. At different chain lengths as shown in Figure 8, the configurational entropy promotes the adsorption of short chains on the wall and the longer chains depart from the wall. Consequently, an increase in density is observed for A but a decrease for B near the wall. At different hard-core diameters as shown in Figure 9, a pronounced difference is observed in the density profiles of A and B. With increasing diameter of B, the density of A remains nearly identical, a wider region near the wall becomes inaccessible to B, and the contact density of B increases. A larger diameter of B leads to a greater repulsive interaction and packing fraction; therefore, the density profiles of B resemble those of hard-sphere fluids. At different wall–fluid interactions as shown in Figure 10, with

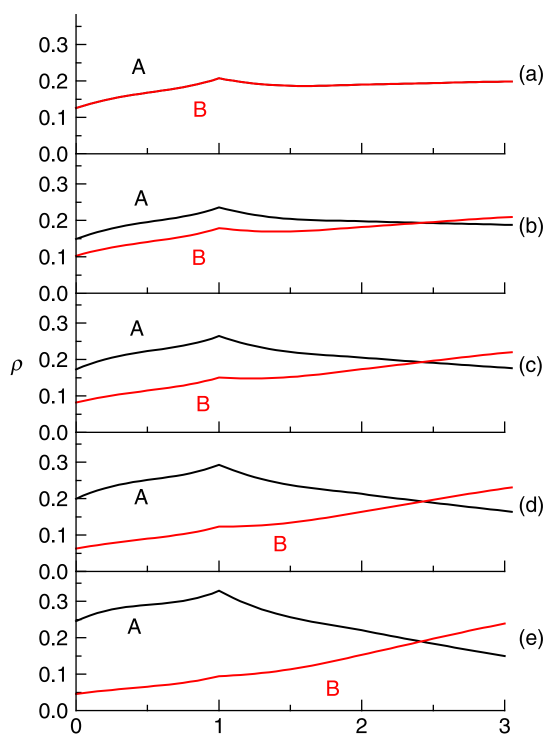

Figure 7. Density profiles of mixtures with the same length (10-mer), same diameter (σ) and same segment density (0.191), but different fluid–fluid interactions: (a) $\beta\varepsilon_{AA} = \beta\varepsilon_{BB} = 0.2$, (b) $\beta\varepsilon_{AA} = 0.15$, $\beta\varepsilon_{BB} = 0.25$, (c) $\beta\varepsilon_{AA} = 0.1$, $\beta\varepsilon_{BB} = 0.3$, (d) $\beta\varepsilon_{AA} = 0.05$, $\beta\varepsilon_{BB} = 0.35$ and (e) $\beta\varepsilon_{AA} = 0.0$, $\beta\varepsilon_{BB} = 0.4$.

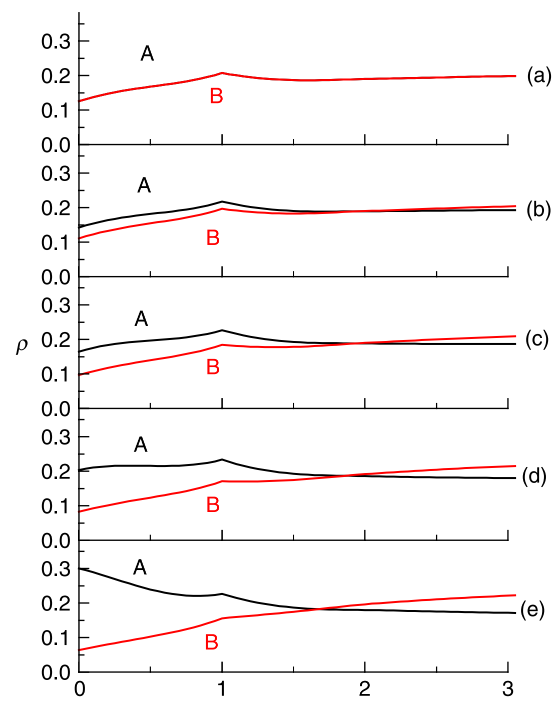

Figure 8. Density profiles of mixtures with the same interaction ($\beta\varepsilon_{AA} = \beta\varepsilon_{BB} = 0.2$), same diameter ($\sigma$) and same segment density (0.191) but different chain lengths: (a) A (10-mer) and B (10-mer), (b) A (8-mer) and B (12-mer), (c) A (6-mer) and B (14-mer), (d) A (4-mer) and B (16-mer) and (e) A (2-mer) and B (18-mer).

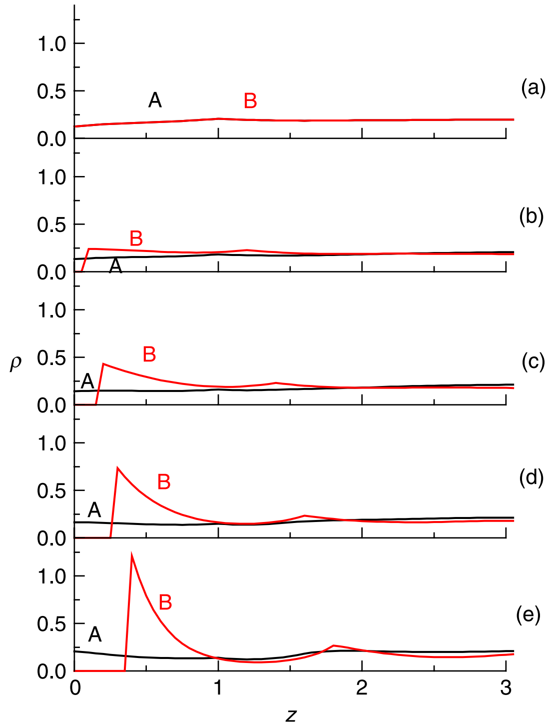

Figure 9. Density profiles of mixtures with the same interaction ($\beta\varepsilon_{AA} = \beta\varepsilon_{BB} = 0.2$), same chain length (10-mer) and same segment density (0.191) but different diameters: (a) A (1.0σ) and B (1.0σ), (b) A (1.0σ) and B (1.1σ), (c) A (1.0σ) and B (1.2σ), (d) A (1.0σ) and B (1.3σ) and (e) A (1.0σ) and B (1.4σ).

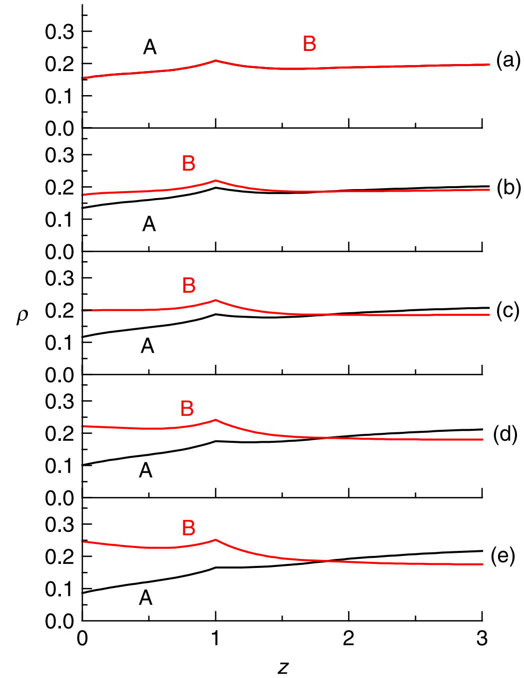

Figure 10. Density profiles of mixtures with the same chain length (10-mer), same diameter (1.0σ), same interaction ($\beta\varepsilon_{AA} = \beta\varepsilon_{BB} = 0.2$) and same segment density (0.191) but different wall–fluid interactions: (a) $\beta\varepsilon_{wA} = \beta\varepsilon_{wB} = 0.2$, (b) $\beta\varepsilon_{wA} = 0.15$, $\beta\varepsilon_{wB} = 0.25$, (c) $\beta\varepsilon_{wA} = 0.1$, $\beta\varepsilon_{wB} = 0.3$, (d) $\beta\varepsilon_{wA} = 0.05$, $\beta\varepsilon_{wB} = 0.35$ and (e) $\beta\varepsilon_{wA} = 0.0$, $\beta\varepsilon_{wB} = 0.4$.

increasing ε_{wB} and decreasing ε_{wA}, B is more densely packed near the wall and A exhibits the opposite behaviour.

4. Conclusions

We have developed a DFT to investigate the structural and thermodynamic properties of Yukawa chain fluids confined between two parallel attractive walls. A simple Heaviside function was used as the weighting function for both repulsive and attractive parts of the excess free-energy functional. The weighting function was truncated at the hard-core diameter for the repulsive part and at r_{cut} for the attractive part. Compared to the simulation data, the DFT provides accurate predictions of density profiles near the wall for Yukawa chain fluids with various chain lengths, densities, fluid–fluid and wall–fluid interactions. Although a simple weighting function was used, our DFT is superior to Goel et al.'s theory with a sophisticated function. The effects of r_{cut} on the predictions of density profiles were examined and an optimal value of r_{cut} was identified. The DFT was also used to predict the surface excess and partition coefficient of pure fluids, and the density profiles of mixtures with different attractive interactions, chain lengths, hard-core diameters and wall–fluid interactions. The use of weighted density approximation in our theory for both repulsive and attractive parts performs well for Yukawa chain fluids and the theory could be extended to more complicated systems.

Acknowledgements

This work was supported by the National Natural Science Foundation of China (Project Nos 20676030 and 20736002), Program for Changjiang Scholars and Innovative Research Team in University (No. IRT0721) and the 111 Project (No. B08021).

References

[1] D. Henderson (ed.), *Fundamentals of Inhomogeneous Fluids*, Marcel Dekker, New York, 1992.
[2] D. Nicholson and N.G. Parsonage, *Computer Simulation and the Statistical Mechanics of Adsorption*, Academic, New York, 1982.
[3] M.P. Allen and D.J. Tildesley, *Computer Simulation of Liquids*, Clarendon, Oxford, 1987.
[4] R. Dickman and C.K. Hall, *High density Monte Carlo simulations of chain molecules: Bulk equation of state and density profile near walls*, J. Chem. Phys. 89 (1988), pp. 3168–3174.
[5] S.K. Kumar, M. Vacatello, and D.Y. Yoon, *Off-lattice Monte Carlo simulations of polymer melts confined between two plates*, J. Chem. Phys. 89 (1988), pp. 5206–5215.
[6] G.F. Tuthill, *Computer simulations of two-dimensional flexible polymers in the dense phase*, J. Chem. Phys. 90 (1989), pp. 5869–5872.

[7] A. Yethiraj and C.K. Hall, *Behavior of starlike polymers between walls*, Macromolecules 24 (1991), pp. 709–713.
[8] A. Yethiraj, *Entropic and enthalpic surface segregation from blends of branched and linear polymers*, Phys. Rev. Lett. 74 (1995), pp. 2018–2021.
[9] A. Yethiraj, *A Monte Carlo simulation study of branched polymers*, J. Chem. Phys. 125 (2006), p. 204901.
[10] G. Rickayzen and A. Augousti, *Integral-equations and the pressure at the liquid–solid interface*, Mol. Phys. 52 (1984), pp. 1355–1366.
[11] N. Choudury and S.K. Ghosh, *Colloidal dispersion confined in a planar slit: A density functional approach*, J. Chem. Phys. 104 (1996), pp. 9563–9568.
[12] O. Pizio and A. Partykiejew, *Evaluation of liquid–vapor density profiles for associating fluids in pores from density functional theory*, J. Chem. Phys. 113 (2000), pp. 10761–10767.
[13] Y. Rosenfeld, *Free-energy model for the inhomogeneous hard-sphere fluid mixture and density functional theory of freezing*, Phys. Rev. Lett. 63 (1989), pp. 980–983.
[14] M. Schmidt, *Density functional theory for soft interactions by dimensional crossover*, Phys. Rev. E 60 (1999), pp. R6291–R6294.
[15] A. González and J.A. White, *Density functional theory of fluids in nanopores: Analysis of the fundamental measures theory in extreme dimensional-crossover situations*, J. Chem. Phys. 125 (2006), p. 064703.
[16] S.Q. Zhou and E. Ruckenstein, *A density functional theory based on the universality of the free energy density functional*, J. Chem. Phys. 112 (2000), pp. 8079–8082.
[17] A. Yethiraj and C.E. Woodward, *Monte Carlo density functional theory of nonuniform polymer melts*, J. Chem. Phys. 102 (1995), pp. 5499–5505.
[18] A. Yethiraj, *Density functional theory of polymers: A Curtin–Ashcroft type weighted density approximation*, J. Chem. Phys. 109 (1998), pp. 3269–3275.
[19] W.A. Curtin and N.W. Ashcroft, *Weighted-density-functional theory of inhomogeneous liquids and the freezing transition*, Phys. Rev. A 32 (1985), pp. 2909–2919.
[20] C.N. Patra and A. Yethiraj, *Generalized van der Waals density functional theory for nonuniform polymers*, J. Chem. Phys. 112 (2000), pp. 1579–1584.
[21] C.N. Patra and A. Yethiraj, *Density functional theory for nonuniform polymers: Accurate treatment of the effect of attractive interactions*, J. Chem. Phys. 118 (2003), pp. 4702–4706.
[22] J.G. Curro and K.S. Schweizer, *PRISM theory of the structure, thermodynamics, and phase-transitions of polymer liquids and alloys*, Adv. Polym. Sci. 116 (1994), pp. 319–377.
[23] T. Goel and C.N. Patra, *Effect of attractive interactions on the structure of polymer melts confined between surfaces: A density functional approach*, J. Chem. Phys. 122 (2005), p. 214910.
[24] Z.C. Ye, J. Cai, H.L. Liu, and Y. Hu, *Density and chain conformation profiles of square-well chains confined in a slit by density functional theory*, J. Chem. Phys. 123 (2005), p. 194902.
[25] Z.C. Ye, H.Y. Chen, J. Cai, H.L. Liu, and Y. Hu, *Density functional theory of homopolymer mixtures confined in a slit*, J. Chem. Phys. 125 (2006), p. 124705.
[26] E.M. del Río, A. Galindo, and E. de Miguel, *Density functional theory and simulation of the columnar phase of a system of parallel hard ellipsoids with attractive interactions*, Phys. Rev. E 72 (2005), p. 051707.
[27] Z.D. Li and J.Z. Wu, *Density functional theory for the structures and thermodynamic properties of highly asymmetric electrolyte and neutral component mixtures*, Phys. Rev. E 70 (2004), p. 031109.
[28] Z.D. Li, D.P. Cao, and J.Z. Wu, *Density functional theory and Monte Carlo simulation for the surface structure and correlation functions of freely jointed Lennard-Jones polymeric fluids*, J. Chem. Phys. 122 (2005), p. 174708.
[29] A. Ayadim and S. Amokrane, *Phase transitions in highly asymmetric binary hard-sphere fluids: Fluid–fluid binodal from a two-component mixture theory*, Phys. Rev. E 74 (2006), p. 021106.
[30] Y. Martínez-Ratón, J.A. Capitan, and J.A. Cuesta, *Fundamental-measure density functional for mixtures of parallel hard cylinders*, Phys. Rev. E 77 (2008), p. 051205.
[31] B. Peng and Y.X. Yu, *A density functional theory for Lennard-Jones fluids in cylindrical pores and its applications to adsorption of nitrogen on MCM-41 materials*, Langmuir 24 (2008), pp. 12431–12439.
[32] S. Karanikas, J. Dzubiella, A. Moncho-Jordá, and A.A. Louis, *Density profiles and solvation forces for a Yukawa fluid in a slit pore*, J. Chem. Phys. 128 (2008), p. 204704.
[33] S.C. Kim and S.H. Lee, *Weighted-density approaches for polymer structure at solid-polymer interfaces*, Mol. Phys. 103 (2005), pp. 1875–1884.
[34] Z. Yang and X.N. Yang, *Structure of hard-core Yukawa fluid mixtures near a semi-permeable membrane: A density functional study*, J. Membr. Sci. 320 (2008), pp. 381–389.
[35] T. Jiang and J.Z. Wu, *Ionic effects in collapse of polyelectrolyte brushes*, J. Phys. Chem. B 112 (2008), pp. 7713–7720.
[36] T. Jiang, Z.D. Li, and J.Z. Wu, *Structure and swelling of grafted polyelectrolytes: Predictions from a nonlocal density functional theory*, Macromolecules 40 (2007), pp. 334–343.
[37] Z.D. Li and J.Z. Wu, *Density functional theory for polyelectrolytes near oppositely charged surfaces*, Phys. Rev. Lett. 96 (2006), p. 048302.
[38] H.L. Liu and Y. Hu, *Molecular thermodynamic theory for polymer systems. II. Equation of state for chain fluids*, Fluid Phase Equilib. 122 (1996), pp. 75–97.
[39] A. Gil-Villegas, A. Galindo, P.J. Whitehead, S.J. Mills, G. Jackson, and A.N. Burgess, *Statistical associating fluid theory for chain molecules with attractive potentials of variable range*, J Chem. Phys. 106 (1997), pp. 4168–4186.
[40] W.E. McMullen and K.F. Freed, *A density functional theory of polymer phase transitions and interfaces*, J. Chem. Phys. 92 (1990), pp. 1413–1426.
[41] C.E. Woodward, *A density functional theory for polymers: Application to hard chain–hard sphere mixtures in slitlike pores*, J. Chem. Phys. 94 (1991), pp. 3183–3191.
[42] J.B. Hooper, J.D. McCoy, J.G. Curro, and F. van Swol, *Density functional theory of simple polymers in a slit pore. III. Surface tension*, J. Chem. Phys. 113 (2000), pp. 2021–2024.

Appendix: SAFT-VR EOS for Yukawa chain fluids

In SAFT-VR EOS, the excess free energy for the Yukawa chain fluid can be expressed as

$$\frac{\mathrm{A}^{\mathrm{ex}}}{NkT}=\frac{\mathrm{A}^{\mathrm{mono}}}{NkT}+\frac{\mathrm{A}^{\mathrm{chain}}}{NkT},$$

where

$$\frac{\mathrm{A}^{\mathrm{mono}}}{NkT}=ma^{\mathrm{M}} \quad \text{and} \quad \frac{\mathrm{A}^{\mathrm{chain}}}{NkT}=-(m-1)\ln y^{\mathrm{M}}(\sigma),$$

in which m is the chain length and σ is the diameter of the segment.

For monomer contribution,

$$a^{\mathrm{M}}\approx a^{\mathrm{HS}}+\beta a_1+\beta^2 a_2,$$

in which

$$a^{\mathrm{HS}}=\frac{4\eta-3\eta^2}{(1-\eta)^2}$$

and

$$a_1=-12\eta\varepsilon(\lambda^{-1}+\lambda^{-2})\frac{1-\eta_{\mathrm{eff}}/2}{(1-\eta_{\mathrm{eff}})^3},$$

where

$$\eta_{\mathrm{eff}}(\eta,\lambda)=c_1\eta+c_2\eta^2,$$

$$\begin{pmatrix} c_1 \\ c_2 \end{pmatrix}=\begin{pmatrix} 0.900678 & -1.50051 & 0.776577 \\ -0.314300 & 0.257101 & -0.0431566 \end{pmatrix}\times\begin{pmatrix} 1 \\ \lambda^{-1} \\ \lambda^{-2} \end{pmatrix},$$

and

$$a_2=\frac{1}{2}\varepsilon\frac{(1-\eta)^4}{(1+2\eta)^2}\eta\frac{\partial a_1^*(\lambda)}{\partial\eta},$$

where

$$a_1^*=-6\eta\varepsilon\lambda^{-1}\frac{1-\eta^*/2}{(1-\eta^*)^3},$$

$$\eta^*(\eta,\lambda)=d_1\eta+d_2\eta^2,$$

$$\begin{pmatrix} d_1 \\ d_2 \end{pmatrix}=\begin{pmatrix} 0.989601 & -0.872203 & 0.320808 & 0.0 & 0.0 \\ -0.0119152 & -1.24029 & 2.41636 & -2.01922 & 0.647565 \end{pmatrix}\times\begin{pmatrix} 1 \\ \lambda^{-1} \\ \lambda^{-2} \\ \lambda^{-3} \\ \lambda^{-4} \end{pmatrix}.$$

For the chain contribution,

$$y^{\mathrm{M}}(\sigma)=g^{\mathrm{Y}}(\sigma^+)\exp(-\beta\varepsilon),$$

in which

$$g^{\mathrm{Y}}(\sigma^+)=g^{\mathrm{HS}}(\sigma^+)+\frac{1}{4}\beta\left[\frac{\partial a_1}{\partial\eta}+\frac{\lambda}{3\eta}\frac{\partial a_1}{\partial\eta}-\frac{1+\lambda}{3\eta}a_1\right],$$

$$g^{\mathrm{HS}}(\sigma^+)=\frac{1-\eta/2}{(1-\eta)^3}.$$